Synthesis and Characterization of Ag_2O, $CoFe_2O_4$, GO and their ternary composite for antibacterial activity

Komal Aftab
COMSATS University Islamabad
Taiba Naseem
University of Azad Jammu and Kashmir
Shahzad Hussain
COMSATS University Islamabad
Sirajul Haq
University of Azad Jammu and Kashmir
Mahfooz Ur Rehman
Hazara University Mansehra Pakistan
Muhammad Waseem (waseem_atd@yahoo.com)
COMSATS University Islamabad https://orcid.org/0000-0002-6118-8057

Research Article

Keywords: Antibacterial, Cobalt ferrite, GO, Silver oxide, Ternary composite

Posted Date: February 28th, 2022

DOI: https://doi.org/10.21203/rs.3.rs-1269336/v1

Abstract

Currently, nanomaterials with exceptional antibacterial activity have become an emerging domain in research. The optimization of nanomaterials against infection causing agents is the next step in dealing with the present-day problem of antibiotics. In this research work, Ag_2O, $CoFe_2O_4$, and $Ag_2O/CoFe_2O_4/rGO$ are prepared by chemical methods. The structural and morphological properties were studied by UV-Vis spectroscopy, X-ray diffraction spectroscopy (XRD), scanning electron microscopy (SEM), energy dispersive X-ray spectroscopy (EDX), and Fourier-transform infrared (FTIR) spectroscopy. The synthesized Ag_2O, $CoFe_2O_4$, and $Ag_2O/CoFe_2O_4/rGO$ nanomaterials were used for antibacterial activities. The nanomaterials were investigated for antibacterial properties, and results showed that all these materials exhibit superior antibacterial efficacy against gram-positive strains like *Staphylococcus aureus* (*S. aureus*) and gram-negative bacterial strains like *Escherichia coli* (*E. coli*). According to the antibacterial results, the nanocomposite significantly reduced the reproduction rate of *E. coli* and *S. aureus*. Moreover, the antibacterial activity of nanomaterials showed a gradual increment with an increase in the concentration of the materials. These results demonstrate that all the nanomaterials, as a kind of antibacterial material, have a great potential for application in a wide range of biomedical applications.

1. Introduction

According to the US Centers for Disease Control and Prevention (CDC), more than 33,000 deaths are attributed to infections with antibiotic-resistant bacteria in the European Union alone. Tragically, the human world is standing at the threshold of a “post-antibiotic era”, where the toll of death from bacterial infection will be greater than that of cancer, as stated by the CDC. (Cassini et al. 2019). The unguided and unchecked use of antibiotics is to be blamed for the pathetic situation we are facing today. The evolution of antibacterial resistance and the appearance of genetically mutated resistant bacteria are the main causes of new infections (Christaki et al. 2019). Due to the worldwide rise of drug-resistant bacterial pathogens, the efficacy of conventional antibiotics is falling. Failure of antibiotics is an increasingly urgent problem to humanity leading to lack of therapy for serious infections (Aslam et al. 2018). Even if a new antibiotic is launched, the resistance of bacteria appears. Alternative strategies need to be found as soon as possible. Since antibiotic-resistant bacteria have increased dramatically, there is a need for alternate strategies and new antibacterial agents that can fight against these resistant bacterial strains (Gupta et al. 2019).

Development of novel antibiotic agents has become an essential with the continuous emergence of bacterial resistance. Nanomaterials cause lethal injuries to the pathogens by acquiring a number of different mechanisms (Gao and Zhang 2020). A number of nanomaterial-based antimicrobials have been reported. Among these agents, metallic NPs are very significant due to their strong antibacterial activity. Metal nanoparticles are one of the most promising tools to combat pathogenic elements. They have shown broad spectrum antibiotic activity against various fungal species, mycobacteria, and gram positive and gram negative bacteria(Slavin et al. 2017). Various nanoparticles have been reported to show antibacterial properties against different bacterial species. Silver (Ag), gold (Au), copper (Cu), cobalt

(Co), zinc (Zn) and titanium (Ti) metals, as well as oxides and ferrites of different metals, have been reported to exhibit an antimicrobial effect (Sánchez-López et al. 2020). Different types of nanoparticles show different levels of antibiotic activity. Their unique physical and chemical properties can lead to fine-tuned interactivity between them and bacteria. Graphene derivatives have also been reported to show antibacterial activity, which suggests that they could hold a high place in the biomedical field (Kumar et al. 2019)(Cao et al. 2021).

Stanić and Tanasković reported that silver metal has the strongest antimicrobial effect among metals. (Stanić and Tanasković 2020). Silver oxide comes under metal oxide nanoparticles and is world-known for having extensive applications in a number of fields such as: optical devices, cancer therapy, biological, electrochemical, sensors, catalytic reduction and cosmetics (Tafida et al. 2020)(ur Rahman et al. 2020)(Maheshwaran et al. 2020)(Rashmi et al. 2020)(Ahmed et al. 2020)(Iqbal et al. 2020). Silver oxide (Ag_2O) nanoparticles is also known for its strength in decoloring dyes and for cleaning organic pollution from water. (Rahnama et al. 2021)(Zhou et al. 2020). Cobalt ferrite ($CoFe_2O_4$) NPs, with their unique crystal lattice organization, offer prominent magnetic properties such as magnetic anisotropy, saturation magnetization, coercivity, etc. Because of their enhanced magnetic properties, they can be used in drug delivery, imaging and diagnostics, magnetic hyperthermia, magnetic extraction, separation, and biosensors (Srinivasan et al. 2018)(Amira Alazmi et al. 2019)(Fayazzadeh et al. 2020)(Ghiasi and Malekpour 2020)(Vajedi and Dehghani 2020). As it is rich in structural defects, rGO nanosheets show more interaction with bacteria. In fighting with the bacteria, the mechanism of rGO is similar to that of graphene and GO, i.e., by causing membrane oxidative stress and rupturing. Sharp nanosheets of GO and rGO cause membrane stress, leading to high antibacterial activities and fragmentation of DNA due to an increase in reactive oxygen species ROS (Shi et al. 2016).

To enhance the antibiotic power of nanoparticles combinational approach provides us a pathway where bacteria find it hard to form resistance. Binary and ternary hetero-materials increases surface area and thus improve the antibacterial efficiency in comparison to unary nanomaterials. The ternary heterojunction can magnify the antimicrobial power, further more binary metal nanocomposites (Wang et al. 2017). Recently there is a heightened interest in magnetic nanoparticles for biomedical applications. magnetic nanoparticles with bactericidal effect have been studied (Ning et al. 2020)(Shatan et al. 2019). Cobalt ferrite has been studied for its magneto-antibacterial properties (Meidanchi 2020).

In this paper, Ag_2O and $CoFe_2O_4$ NPs were fabricated using facile chemical reduction and a modified solvothermal technique, respectively. A modified Hummers' method was employed for GO synthesis. A novel ternary nanocomposite $Ag_2O/CoFe_2O_4$/rGO is synthesized by a simple two-step process. The synthesized materials were characterized using UV-Visible spectroscopy, X-ray diffraction (XRD) technique, scanning electron microscopy (SEM), and energy-dispersive X-ray spectroscopy, Fourier-transform infrared (FTIR) spectroscopic technique, and energy-dispersive X-ray (EDX) spectroscopy. The nanomaterials were investigated for their antimicrobial potential against *Staphylococcus aureus* and

Escherichia coli. The union of magnetism, biocompatibility, and nano-knife effect of rGO would make the $Ag_2O/Cofe_2O_4$/rGO ternary nanocomposite a technically brilliant material in biomedical applications.

2. Methodology

2.1. Reagents

All chemicals were analytically pure and were used without further purification. Sodium borohydride [$NaBH_4$, Sigma-Aldrich]: Ethylene glycol [$C_2H_6O_2$, Analar]; Sodium hydroxide [NaOH, Sigma-Aldrich]; Iron trichloride hexahydrate [$FeCl_3.6H_2O$, 98% BDH Analar]; Graphite powder [99%, Sigma-Aldrich]; Phosphoric acid [H_3PO_4, Fischer Scientific]; Cobalt chloride hexahydrate [$CoCl_2.6H_2O$, 98% MERCK]; Sodium acetate [$Na(CH_3COO$, 99% Sigma-Aldrich]; Potassium permanganate [$KMnO_4$, 97%, Sigma-Aldrich]; Silver nitrate [$AgNO_3$, Sigma-Aldrich]; Hydrogen peroxide [H_2O_2, 30 wt.% in H_2O Sigma-Aldrich]; Sulphuric acid [H_2SO_4, 95–98%, Fischer scientific]; Ethanol [C_2H_5OH, Analar]; and Deionized (DI) water.

2.2. Synthesis of Silver Oxide Nanoparticles

Simple wet chemical approach was used to synthesize nanoparticles of silver oxide. In this method, firstly a solution of silver nitrate was prepared. 150 mL of 10 mM solution of $AgNO_3$ was heated up to 70°C and 0.056 g of sodium borohydride was added to this solution of silver salt slowly. The mixture was kept stirring while the temperature being maintained at 70° C. After five minutes 10 mL of freshly prepared 0.2 M NaOH was added which lead to formation of, black-brown precipitates. The mixture was stirred for half an hour. After 24 hours aging, the precipitates were washed using DI water till neutral pH was obtained and then dried at 110°C.

2.3. Synthesis of Cobalt Ferrite Nanoparticles

A modified solvothermal technique was used to obtain cobalt ferrite nanoparticles. Ethylene glycol was selected as the solvent. 0.405 g of $FeCl_3.6H_2O$ and 0.178 g of $CoCl_2.6H_2O$ were used to form a solution in 150 mL of ethylene glycol (EG) by sonicating the mixture for one hour. After sonication, the colour turned bright orange. Then, 6.15 g of sodium acetate was put in the solution, and it was magnetically stirred for another hour, and the mixture gave a reddish orange tint. The mixture was poured into a 200 mL Teflon autoclave and placed in the oven for four hours at 180°C. Precipitates were collected, washed using DI water, and then dried at 110°C.

2.4. Synthesis of Graphene Oxide

Graphite powder was used as a precursor for the synthesis of GO by utilizing the well-known modified Hummer's method. Firstly, in an ice bath, 90 mL of H_2SO_4 was mixed with 10 mL of 29 H_3PO_4 (volume ratio of 9:1) and mixed using a magnetic stirrer for some time at 10°C. In this mixture, 0.75 g of graphite powder was introduced while being stirred and kept in an ice bath. When it was homogenized, 4.5 g of $KMnO_4$ was added gradually. After the addition of $KMnO_4$, it was kept stirring for six hours without

disruption. This resulted in a dark green slurry. The dropwise addition of 0.75 mL of H_2O_2 leads to the removal of excess $KMnO_4$. The mixture was stirred for another 10 minutes. As a result of the H_2O_2 addition, an exothermic reaction occurred, and an ice bath was used to cool it down. Upon cooling, 25 mL of HCl was added, followed by 75 mL of DI water. The resultant suspension was centrifuged and washed at 12000 rpm till a neutral pH was obtained. The washed GO was dried in the oven for 24 hours at 60°C. After this, the dried GO obtained was then ground to obtain a fine GO powder (Fig. 1).

2.5. Synthesis of $Ag_2O/CoFe_2O_4$/rGO Nanocomposite

$Ag_2O/CoFe_2O_4$/rGO nanocomposite was prepared by the two-step approach reaction of $AgNO_3$, $CoCl_2{\cdot}6H_2O$, $FeCl_3{\cdot}6H_2O$ and GO. Firstly, in 100 mL of ethylene glycol, 100 mg of GO was dispersed by ultrasonically treating the mixture for one hour. Next 8 mg of $AgNO_3$ was put into the suspension and then magnetically stirred so that homogeneous solution was obtained. Into this system, 100 mL of $NaBH_4$/EG (38 mg/mL) was dropped. Magnetic stirrer was used to stir the mixture. Few minutes later, precipitates were obtained. After centrifugation, the precipitates of Ag_2O/rGO nanocomposite were washed and separated for further use. Subsequently, for the preparation of $Ag_2O/CoFe_2O_4$/rGO ternary nanocomposite, 8 mg of $CoCl_2{\cdot}6H_2O$ and 20 mg of $FeCl_3{\cdot}6H_2O$ were dispersed in 70 mL of EG. Next, 2.38 g of sodium acetate was added. After this, magnetic stirring was performed for half an hour. Then as prepared Ag_2O/rGO nanocomposite was added while vigorously stirring the solution. The mixture was shifted to a stainless-steel based autoclave (Teflon-lined) and kept for 4 hours in oven at 180°C. Then centrifuged and washed several times before drying in oven at 110°C.

2.6. Characterization

The synthesized nanomaterials were characterized using UV–Vis, XRD, SEM, EDX, DLS, and FT-IR spectroscopic analysis. The synthesized nanomaterials were characterized by a UV-Vis spectrophotometer (1601 Shimadzu). An X-ray diffractometer (JDX-3532 (JEOL), Japan), over the 2θ range of 10-80°, was used to analyse phase structures with radiation at 40 kV and 20 mA. The SEM model used was JSM 5910 (JEOL), Japan. On a double stick tape, first the samples were deposited and then placed in an aluminium sample holder. Before analysis, they were also sputter-coated in gold in a sputter coater model SPI-Module (USA) at 30 mA for 90 seconds. The instrument used for this technique was an EDX microanalyzer model INCA 200 (UK).

2.7. Antibacterial Assay

Antibacterial activities were performed against the selected bacterial strains using the synthesized nanomaterials. In this study, gram positive bacteria "*Staphylococcus aureus*" and gram-negative "*Escherichia coli*" were selected for anti-bacterial activity. An agar well diffusion assay was used in order to obtain a qualitative evaluation of the antibacterial effects of synthesized materials. Agar solution was prepared and spread on the plates, and then bacterial cultures were placed on the plates using a cotton swab. After that, three holes (3 mm in size) were punched in the plate by a sterilized cork borer. Levofloxacin was used as a standard material. Each of the three holes received 10 µL of 500 g/mL Ag_2O,

1 mg/L Ag_2O, and standard antibiotic. To avoid the spillage of the solution over the plate, extreme care was taken. More plates were prepared in which $CoFe_2O_4$ and $Ag_2O/CoFe_2O_4$/rGO were added in the same way. The plates were then placed in an incubator for incubation for 24 hours at 36°C. After that, the zone of inhibition was measured and noted after a growth period of 24 hours.

3. Results And Discussion

3.1. Characterization

3.1.1. X- ray Diffraction Analysis

XRD results of synthesized material are presented in Fig. 2. For each of them, the particle size of nanocomposite has been calculated by Scherrer formula:

$D = 0.89\lambda/\beta Cos\theta$ (1)

Where “θ” shows Bragg angle, “β” is full width half maximum and “λ” shows wavelength of X-rays used during the diffraction process.

The 2θ value observer for the synthesized silver oxide are 34.83°, 43.65°, 63.03°, 67.75° and 75.87°. These diffraction peaks belong to the 111, 200, 220 and 311 crystal planes. The crystallite size calculated using Scherrer equation is 14 nm approximately. Similar findings were reported by Sangappa et al. (Sangappa and Thiagarajan 2015). The diffraction peaks observed are in perfect match with the JCPDS card no. 76-1393. Cobalt ferrite showed diffraction peaks 18.0°, 29.6°, 35.4°, 43.0°, 53.0°, 56.6° and 62.2° 2θ values. These peaks can be assigned to (111), (220), (311), (400), (422), (511) and (440) crystal planes of $CoFe_2O_4$, respectively. The observed XRD peaks were indexed to a cubic crystal structure. The results are found to be in consistence with the reported data (Wang et al. 2015). The crystallite size calculated for the nanoparticles was found to be 5 nm approximately. The diffraction peaks observed are in perfect match with the JCPDS card no. 22-1086. For GO, 10.15° 2θ value is observed. The lattice spacing for graphene oxide is found to be 0.87 nm. The results are found to be close to that reported by Bahrami et al. where the peak was found to be at 10. 31°. However, there was another peak that showed the partial reduction of GO into rGO. No such peak is observed in the XRD spectrum of GO (Bahrami et al. 2019). The 2θ peaks observed in the synthesized ternary nanocomposite are 24.4° and 43.36°. The two broad peaks correspond to the rGO. No peaks are visible for the other two components. The reason mainly is the much smaller quantity of silver oxide and cobalt ferrite. The peaks are totally masked by the two broad peaks of rGO or due to their very small intensity as compared to that of rGO peaks they are not visible. The small content of these two components is also visible from the EDX of the material.

3.1.2. UV-Visible Spectroscopy

UV-Visible spectroscopy was performed for each nanomaterial synthesized (Fig. 3). The band gap energy is also determined from these absorbance spectra by using Tauc method based on the assumption that

energy-dependent absorption coefficient α can be expressed as:

$(\alpha \cdot hv)^{1/\gamma} = B\,(hv - E_g)$ $(\alpha \cdot hv)^{1/\gamma} = B\,(hv - E_g)$ (2)

Here, *h* is Planck constant, E_g means band gap energy, v denotes photon's frequency and *B* is a constant. In this equation γ factor is dependent on nature of electron transition and its value is 1/2 for direct and 2 for indirect transition band gaps (Makuła et al. 2018). The UV-Vis spectroscopy was performed from 300 to 800 nm range. The maxima for silver oxide was found to be at 410 nm while it was reported 430 nm by Shume and coworkers (Shume et al. 2020). For silver oxide, band gap was 1.83 eV. The band gap of Ag_2O can lie in a wide range of 1.2 to 3.4 eV (Makuła et al. 2018). For cobalt ferrite, the absorption maxima is found to be at 348 nm (Nithiyanantham et al. 2021). The band gap was measured equal to 2.44 eV which is near 2.273 eV found by Yuliantika (Yuliantika et al.). GO showed one absorption peak at 230 nm and another shoulder at 270 nm. Gurunanthan and co-workers also reported an peak at 230 nm while the shoulder was seen at almost 300 nm (Gurunathan et al. 2012). The band gap was found to be 4.3 eV. The ternary nanocomposite showed absorption at 260, 340 and 385 nm. The peaks may be attributed to rGO, cobalt ferrite and silver oxide. The band gap was found to be 2.05 eV.

3.1.3. Scanning Electron Microscopy

Figure 4 represents the SEM images of silver oxide, $CoFe_2O_4$, GO and their ternary system. The scanning electron micrograph of silver oxide suggests that the surface morphology of silver oxide, is quite uniform and very well-defined. The nanoparticles of silver oxide are almost spherical in shape (Banua and Han 2020). The SEM images of $CoFe_2O_4$ reflects the grown NPs are well developed, with uniform morphology. The figure depicts the homogeneous size distribution of particles that makes sure its nano-crystalline nature. Due to the magnetic interactions and high surface energy of $CoFe_2O_4$ nanoparticles, aggregation of NPs was seen (Ensafi et al. 2017). The micrograph of GO shows the surface morphology reveals that GO consisted of many flakes having both crumpled and stacked ones. There were also closely associated cavities present. It was observed that wrinkles were present across GO layer because of its crumpling nature (Iqbal et al. 2020). In the SEM image of the ternary nanocomposite, the sheets of the reduced graphene oxide can be seen twisted and folded with a rough structure. Wrinkling on rGO was present because of the rapid removal of oxygen-containing functional groups in GO. Due to their entrapment inside the crumpled rGO sheets, the nanoparticles are not very visible.

3.1.4. Energy-dispersive X-ray spectroscopy

EDX was performed to determine the elemental composition of the prepared materials (Fig. 5). The EDX spectrum of silver oxide showed a larger amount of silver and oxygen than expected, which indicates the formation of Ag_2O. No impurities on the surface of the nanoparticles were found, showing the purity of the synthesized nanoparticles. In the EDX spectrum of cobalt ferrite, the major presence of Co, Fe, and oxygen is obvious. Some other elements are seen present on the surface of the particles that might come from the precursors used. From the elemental percentage, a high ratio of cobalt, iron, and oxygen can be seen. The EDX spectrum of the synthesized ternary nanocomposite shows the presence of all constituent

elements: carbon, oxygen, silver, cobalt, and iron. As impurities, a small amount of sodium and silicon are also present. The intensity of metal peaks is small due to their smaller ratio, which is also clear from their weight percentage.

3.1.5. FTIR Spectroscopy

The FTIR spectra (Fig. 6) clearly defines the absorption bands detected in the samples. Prominent bands for silver oxide were seen at 3380 cm^{-1} and 545 cm^{-1}. Among these the bands at 3380 cm^{-1} corresponds to H-O-H stretching vibration of water molecules. FTIR spectrum of synthesized Ag_2O nanoparticles displays the characteristic band due to lattice vibration of silver oxide at 545 cm^{-1} (approx.) which shows the successful synthesis of silver oxide. The band near 1380 cm^{-1} may correspond to nitrate vibrations. The metal–oxygen stretching frequencies are observable in the range of 500 to 600 cm^{-1} (Ravichandran et al. 2016)(Shume et al. 2020). The band at 545 cm^{-1} is very close to one reported by Siddiqui et al. i.e. 550 cm^{-1} (Siddiqui et al. 2013). This further verified the compounds as silver oxide particles in addition to the XRD analysis conducted. The remaining bands are present due to silver nitrate (Yong et al.). In the FTIR spectra of cobalt ferrite, bands at 3433, 1635, 619, and 447 cm^{-1} were observed. The bands at 3433 cm^{-1} and 1635 cm^{-1} represent the stretching and bending vibration mode of O-H bond by water molecule absorbed by the surface of nanoparticles during the synthesis process.

The bands that appeared at 619 and 447 cm^{-1} represent the characteristic bands of Fe-O and Co-O metal-oxygen bonds which confirms the successful synthesis of $CoFe_2O_4$ nanoparticles. The absorbance bands exhibited the formation of cobalt ferrite phase with spinel structure. As reported by Yuliantika et al, Spinel ferrite has face-centered cubic structure (Yuliantika et al.). The result is in agreement with the findings of Shanmugavel et al. and Oliveira et al (Shanmugavel et al. 2014) (Oliveira et al. 2013). Following bands are observed in the spectrum of GO; 3450, 1716, 1635, 163, 1216 and 1072 cm^{-1}. In this, the characteristic band at 3450 cm^{-1} was because of O-H stretching. At 1716 C=O groups in carboxyl and carbonyl moieties are present. C-C skeletal vibration bands of unoxidized graphitic domains or contribution from the stretching deformation vibration of carboxyl group 1363 cm^{-1}, intercalated water at 1635 cm^{-1}, epoxide C–O–C or phenolic C–O–H stretching vibrations 1216 cm^{-1}, and C–O stretching vibrations in the epoxy or alkoxy groups are represented by the band at 1072 cm^{-1}. These bands confirm the various functional groups like intercalated water, carboxyl group, epoxide, phenolic, and alkoxy groups present on surface of graphene oxide. The results were found to be very close to that reported by Sim et al. (Sim et al. 2014). For the ternary nanocomposite the peak formed at 1728 cm^{-1} represents stretching of C=O of COOH present on the edges of sheet. The decrease in intensity was seen because of the decomposition of the aforementioned groups by hydrothermal treatment. The band at 615 cm^{-1} shows Co-O bond vibration. A very slight band can be seen at 511 cm^{-1} which represents the metal oxygen bond. At 418cm^{-1} stretching vibrations of Fe-O can be seen. 70 The decreased intensities of oxygen containing functional groups confirms conversion of GO into rGO. The metal oxygen bands between 400 to 650 cm^{-1} represents the presence of Ag_2O and $CoFe_2O_4$. The results confirm the formation of the

ternary nanocomposite showing metal-oxygen bonds and reduced graphene oxide. The results are found to be close to that reported by Khan et al. and Iqbal et al (Khan et al. 2020)(Iqbal et al. 2020).

3.2. Antibacterial Activities

The Ag_2O, $CoFe_2O_4$, and $Ag_2O/CoFe_2O_4$/rGO synthesized were tested for antimicrobial efficacy via the Agar well diffusion assay (Fig. 7). The antibacterial efficiency was identified through the appearance of an inhibitory zone around the well. The antibacterial action was studied against gram positive *Staphylococcus aureus* and gram-negative *Escherichia coli* using levofloxacin as a standard. The inhibition against the used bacterial strains was visible after incubation for 24 hours. The figures show the photographs of petri-dishes with different nanomaterials against both the pathogens under study. From the pictures, it is obvious that all nanomaterials can give a good zone of clearance against all three bacteria. S1 and S2 represent the two concentrations used for the antibacterial activity for these two bacteria, i.e., 500 µg/mL and 1 mg/mL, respectively. The table shows the inhibitory zones in mm. The antibacterial activity against *S. aureus* was found for silver oxide, which has a higher inhibitory power as compared to that of cobalt ferrite and is proven by their zones of inhibition. At 500 µg/mL, Ag_2O shows a zone of inhibition of 4 mm, while there is no zone of clearance seen for $CoFe_2O_4$ at this concentration. After increasing the concentration two times, a significant increase in the zone of clearance is seen. The ZOI for Ag_2O is 13 mm, while the ZOI for $CoFe_2O_4$ is 11 mm, and the ternary nanocomposite $Ag_2O/CoFe_2O_4$/rGO has an inhibition zone of 5 and 14 mm. For *E. coli*, the inhibitory area is a bit reduced due to the smaller susceptibility of these bacteria. The following order is found for the nanomaterials under study against gram positive *S. aureus*, $Ag_2O/CoFe_2O_4$/rGO > Ag_2O > $CoFe_2O_4$.

Table 1
Zone of inhibitions noticed against *S. aureus* and *E. coli*

Sr. No.	Nanomaterials	*S. aureus (ZOI mm)*			*E. coli (ZOI mm)*		
		S1	**S2**	**standard**	**S1**	**S2**	**standard**
1.	Ag_2O	04	13	16	05	12	15
2.	$CoFe_2O_4$	00	11	16	04	12	15
3.	$Ag_2O/CoFe_2O_4$/rGO	05	14	16	06	13	15

4. Conclusion

In this study we synthesized nanoparticles by simple and facile methods. The ternary nanocomposite was synthesized by two step synthetic route. The crystallite size of the synthesized nanomaterial was found to be 14 nm, 5 nm, and 5 nm for Ag_2O, $CoFe_2O_4$, and $Ag_2O/CoFe_2O_4$/rGO respectively with well crystallized structure. UV-visible spectra showed significant changes in the band gap. XRD spectra confirmed the phase purity. SEM showed the surface morphology at different resolutions. Different nanomaterials showed the respective functional groups through FTIR spectroscopy. The nanomaterials

showed effective antibacterial effects against the bacteria under study via agar well diffusion method. The antibacterial effect of the nanomaterials was found to be concentration dependent. Ternary nanocomposite $Ag_2O/CoFe_2O_4$/rGO has high prospect as an antimicrobial agent to reduce the growth of bacteria.

Declarations

Ethical approval

This manuscript does not report studies regarding the participation of human or animals.

Consent to Participate

Not applicable.

Consent to Publish

Not applicable.

Authors Contributions

K.A and T.N: Experimentation, writing the draft and drawing all the figures and interpretation. M. W designed the project. S.H and M. W conceptualize and supervised the whole work. S. H also reviewed and corrected the draft. M.R and S.H performed Antibacterial activity and FTIR spectroscopy respectively.

Funding

Not applicable.

Competing interests

The authors declare that they have no conflict of interest.

Availability of data and materials

Not applicable.

References

1. Ahmed A, Hayat A, Nawaz MH et al (2020) Construction of sponge-like graphitic carbon nitride and silver oxide nanocomposite probe for highly sensitive and selective turn-off fluorometric detection of hydrogen peroxide. J Colloid Interface Sci 558:230–241. https://doi.org/10.1016/J.JCIS.2019.09.109

2. Amira Alazmi V, Singaravelu NM, Batra et al (2019) Cobalt ferrite supported on reduced graphene oxide as a T 2 contrast agent for magnetic resonance imaging. RSC Adv 9:6299–6309. https://doi.org/10.1039/C8RA09476D
3. Aslam B, Wang W, Arshad MI et al (2018) Antibiotic resistance: a rundown of a global crisis. Infect Drug Resist 11:1645. https://doi.org/10.2147/IDR.S173867
4. Bahrami A, Kazeminezhad I, Abdi Y (2019) Pt-Ni/rGO counter electrode: electrocatalytic activity for dye-sensitized solar cell. Superlattices Microstruct 125:125–137. https://doi.org/10.1016/J.SPMI.2018.10.026
5. Banua J, Han JI (2020) Biogenesis of Prism-Like Silver Oxide Nanoparticles Using Nappa Cabbage Extract and Their p-Nitrophenol Sensing Activity. Mol 2020, Vol 25, Page 2298 25:2298. https://doi.org/10.3390/MOLECULES25102298
6. Cao G, Yan J, Ning X et al (2021) Antibacterial and antibiofilm properties of graphene and its derivatives.Colloids Surfaces B Biointerfaces200
7. Cassini A, Högberg LD, Plachouras D et al (2019) Attributable deaths and disability-adjusted life-years caused by infections with antibiotic-resistant bacteria in the EU and the European Economic Area in 2015: a population-level modelling analysis. Lancet Infect Dis 19:56–66. https://doi.org/10.1016/S1473-3099(18)30605-4
8. Christaki E, Marcou M, Tofarides A (2019) Antimicrobial Resistance in Bacteria: Mechanisms, Evolution, and Persistence. J Mol Evol 2019 881 88:26–40. https://doi.org/10.1007/S00239-019-09914-3
9. Ensafi AA, Rezaloo F, Rezaei B (2017) $CoFe_2O_4$/reduced graphene oxide/ionic liquid modified glassy carbon electrode, a selective and sensitive electrochemical sensor for determination of methotrexate. J Taiwan Inst Chem Eng 78:45–50. https://doi.org/10.1016/J.JTICE.2017.05.031
10. Fayazzadeh S, Khodaei M, Arani M et al (2020) Magnetic Properties and Magnetic Hyperthermia of Cobalt Ferrite Nanoparticles Synthesized by Hydrothermal Method. J Supercond Nov Magn 2020 337 33:2227–2233. https://doi.org/10.1007/S10948-020-05490-6
11. Gao W, Zhang L (2020) Nanomaterials arising amid antibiotic resistance. Nat Rev Microbiol 2020 191 19:5–6. https://doi.org/10.1038/s41579-020-00469-5
12. Ghiasi A, Malekpour A (2020) Octyl coated cobalt-ferrite/silica core-shell nanoparticles for ultrasonic assisted-magnetic solid-phase extraction and speciation of trace amount of chromium in water samples. Microchem J 154:104530. https://doi.org/10.1016/J.MICROC.2019.104530
13. Gupta A, Mumtaz S, Li C-H et al (2019) Combatting antibiotic-resistant bacteria using nanomaterials. Chem Soc Rev 48:415–427. https://doi.org/10.1039/C7CS00748E
14. Gurunathan S, Han JW, Abdal Dayem A et al (2012) Oxidative stress-mediated antibacterial activity of graphene oxide and reduced graphene oxide in Pseudomonas aeruginosa. Int J Nanomedicine 7:5901–5914. https://doi.org/10.2147/IJN.S37397
15. Iqbal M, Zain-ul-Abdin, Naseem T et al (2020) Synthesis and Characterization of rGO/Ag_2O Nanocomposite and its Use for Catalytic Reduction of 4-Nitrophenol and Photocatalytic Activity. J

Inorg Organomet Polym Mater. https://doi.org/10.1007/s10904-020-01680-w

16. Khan MAM, Khan W, Ahamed M et al (2020) Silver-Decorated Cobalt Ferrite Nanoparticles Anchored onto the Graphene Sheets as Electrode Materials for Electrochemical and Photocatalytic Applications. ACS Omega 5:31076–31084. https://doi.org/10.1021/acsomega.0c04191
17. Kumar P, Huo P, Zhang R, Liu B (2019) Antibacterial properties of graphene-based nanomaterials. Nanomaterials 9:737
18. Maheshwaran G, Nivedhitha Bharathi A, Malai Selvi M et al (2020) Green synthesis of Silver oxide nanoparticles using Zephyranthes Rosea flower extract and evaluation of biological activities. J Environ Chem Eng 8:104137. https://doi.org/10.1016/J.JECE.2020.104137
19. Makuła P, Pacia M, Macyk W (2018) How To Correctly Determine the Band Gap Energy of Modified Semiconductor Photocatalysts Based on UV–Vis Spectra. J Phys Chem Lett 9:6814–6817. https://doi.org/10.1021/ACS.JPCLETT.8B02892
20. Meidanchi A (2020) Cobalt ferrite nanoparticles supported on reduced graphene oxide sheets: optical, magnetic and magneto-antibacterial studies. Nanotechnology 31:445704. https://doi.org/10.1088/1361-6528/ABA7E2
21. Ning P, Liu CC, Wang YJ et al (2020) Facile synthesis, antibacterial mechanisms and cytocompatibility of Ag–$MnFe_2O_4$ magnetic nanoparticles. Ceram Int 46:20105–20115. https://doi.org/10.1016/J.CERAMINT.2020.05.085
22. Nithiyanantham S, Viviliya S, Anandhan S, Mahalakshmi S (2021) Synthesis and Characterization of Cobalt Ferrite through Co-Precipitation Technique. 10:1871–1876. https://doi.org/10.33263/LIANBS101.18711876
23. Oliveira GE, Clarindo JES, Santo KSE, Souza FG (2013) Chemical modification of cobalt ferrite nanoparticles with possible application as asphaltene flocculant agent. Materials Research. ABM, ABC, ABPol, pp 668–671
24. Rahnama F, Ashrafi H, Akhond M, Absalan G (2021) Introducing Ag_2O-Ag_2CO_3/rGO nanoadsorbents for enhancing photocatalytic degradation rate and efficiency of Congo red through surface adsorption. Colloids Surfaces A Physicochem Eng Asp 613:126068. https://doi.org/10.1016/J.COLSURFA.2020.126068
25. Rashmi BN, Harlapur SF, Avinash B et al (2020) Facile green synthesis of silver oxide nanoparticles and their electrochemical, photocatalytic and biological studies. Inorg Chem Commun 111:107580. https://doi.org/10.1016/j.inoche.2019.107580
26. Ravichandran S, Paluri V, Kumar G et al (2016) A novel approach for the biosynthesis of silver oxide nanoparticles using aqueous leaf extract of Callistemon lanceolatus (Myrtaceae) and their therapeutic potential. J Exp Nanosci 11:445–458. https://doi.org/10.1080/17458080.2015.1077534
27. Sánchez-López E, Gomes D, Esteruelas G et al (2020) Metal-based nanoparticles as antimicrobial agents: An overview. Nanomaterials 10
28. Sangappa M, Thiagarajan P (2015) Combating Drug Resistant Pathogenic Bacteria Isolated from Clinical Infections, with Silver Oxide Nanoparticles. Indian J Pharm Sci 77:151

29. Shanmugavel T, Raj SG, Rajarajan G, Kumar GR (2014) Rapid phase synthesis of nanocrystalline cobalt ferrite. In: AIP Conference Proceedings. American Institute of Physics Inc., pp 496–498
30. Shatan AB, Venclíková K, Zasońska BA et al (2019) Antibacterial Silver-Conjugated Magnetic Nanoparticles: Design, Synthesis and Bactericidal Effect. Pharm Res 2019 3610 36:1–12. https://doi.org/10.1007/S11095-019-2680-X
31. Shi L, Chen J, Teng L et al (2016) The Antibacterial Applications of Graphene and Its Derivatives. Small 12:4165–4184
32. Shume WM, Murthy HCA, Zereffa EA (2020) A Review on Synthesis and Characterization of Ag2O Nanoparticles for Photocatalytic Applications. J. Chem. 2020
33. Siddiqui MRH, Adil SF, Assal ME et al (2013) Synthesis and characterization of silver oxide and silver chloride nanoparticles with high thermal stability. Asian J Chem 25:3405–3409. https://doi.org/10.14233/ajchem.2013.13874
34. Sim LC, Leong KH, Ibrahim S, Saravanan P (2014) Graphene oxide and Ag engulfed TiO_2 nanotube arrays for enhanced electron mobility and visible-light-driven photocatalytic performance. J Mater Chem A 2:5315–5322. https://doi.org/10.1039/c3ta14857b
35. Slavin YN, Asnis J, Häfeli UO, Bach H (2017) Metal nanoparticles: Understanding the mechanisms behind antibacterial activity.J. Nanobiotechnology15
36. Srinivasan SY, Paknikar KM, Bodas D, Gajbhiye V (2018) Applications of cobalt ferrite nanoparticles in biomedical nanotechnology. Nanomedicine 13:1221–1238
37. Stanić V, Tanasković SB (2020) Antibacterial activity of metal oxide nanoparticles. In: Nanotoxicity. Elsevier, pp 241–274
38. Tafida RA, Halimah MK, Muhammad FD et al (2020) Structural, optical and elastic properties of silver oxide incorporated zinc tellurite glass system doped with Sm^{3+} ions. Mater Chem Phys 246:122801. https://doi.org/10.1016/J.MATCHEMPHYS.2020.122801
39. ur Rahman MS, Tahir MA, Noreen S et al (2020) Osteogenic silver oxide doped mesoporous bioactive glass for controlled release of doxorubicin against bone cancer cell line (MG-63): In vitro and in vivo cytotoxicity evaluation. Ceram Int 46:10765–10770. https://doi.org/10.1016/J.CERAMINT.2020.01.086
40. Vajedi F, Dehghani H (2020) A high-sensitive electrochemical DNA biosensor based on a novel ZnAl/layered double hydroxide modified cobalt ferrite-graphene oxide nanocomposite electrophoretically deposited onto FTO substrate for electroanalytical studies of etoposide. Talanta 208:120444. https://doi.org/10.1016/J.TALANTA.2019.120444
41. Wang G, Ma Y, Dong X et al (2015) Facile synthesis and magnetorheological properties of superparamagnetic $CoFe_2O_4$/GO nanocomposites. Appl Surf Sci 357:2131–2135. https://doi.org/10.1016/j.apsusc.2015.09.196
42. Wang L, Hu C, Shao L (2017) The antimicrobial activity of nanoparticles: Present situation and prospects for the future. Int J Nanomedicine 12:1227–1249

43. Yong NL, Yong NL, Ahmad A, Mohammad AWSynthesis and Characterization of Silver Oxide Nanoparticles by a Novel Method
44. Yuliantika D, Taufiq A, Hidayat A et al Exploring Structural Properties of Cobalt Ferrite Nanoparticles from Natural Sand. https://doi.org/10.1088/1757-899X/515/1/012047
45. Yuliantika D, Taufiq A, Hidayat A et al Exploring Structural Properties of Cobalt Ferrite Nanoparticles from Natural Sand Recent citations Exploring Structural Properties of Cobalt Ferrite Nanoparticles from Natural Sand. https://doi.org/10.1088/1757-899X/515/1/012047
46. Zhou Z, Li Y, Li M et al (2020) Efficient removal for multiple pollutants via Ag_2O/BiOBr heterojunction: A promoted photocatalytic process by valid electron transfer pathway. Chinese Chem Lett 31:2698–2704. https://doi.org/10.1016/J.CCLET.2020.07.003

Figures

Figure 1

(a) The process of GO synthesis (b) GO slurry after centrifugation (c), (d) GO after drying.

Figure 2

X-ray diffractograms of Ag_2O, $CoFe_2O_4$, GO and $Ag_2O/CoFe_2O_4$/rGO

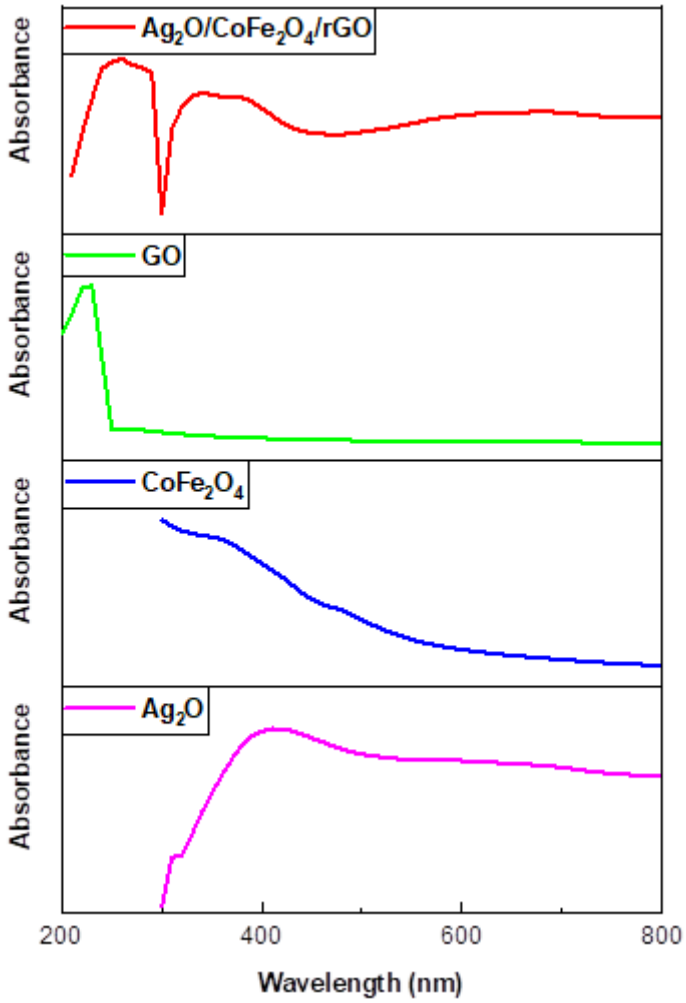

Figure 3

UV-VIS spectra of Ag_2O (pink), $CoFe_2O_4$ (blue), GO (green) and $Ag_2O/CoFe_2O_4$/rGO (red)

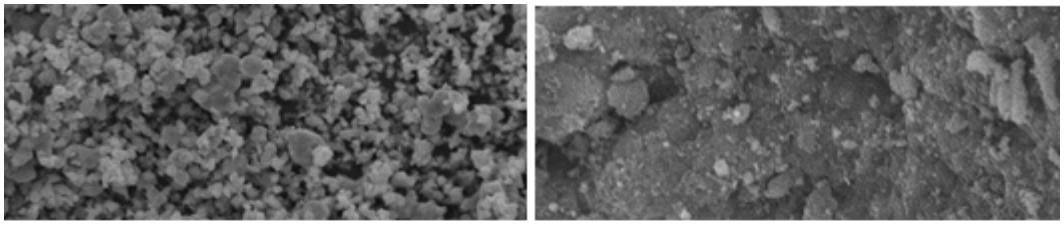

Figure 4

SEM micrograph of (a) Ag_2O (b) $CoFe_2O_4$ (c) GO and (d) $Ag_2O/CoFe_2O_4$/rGO

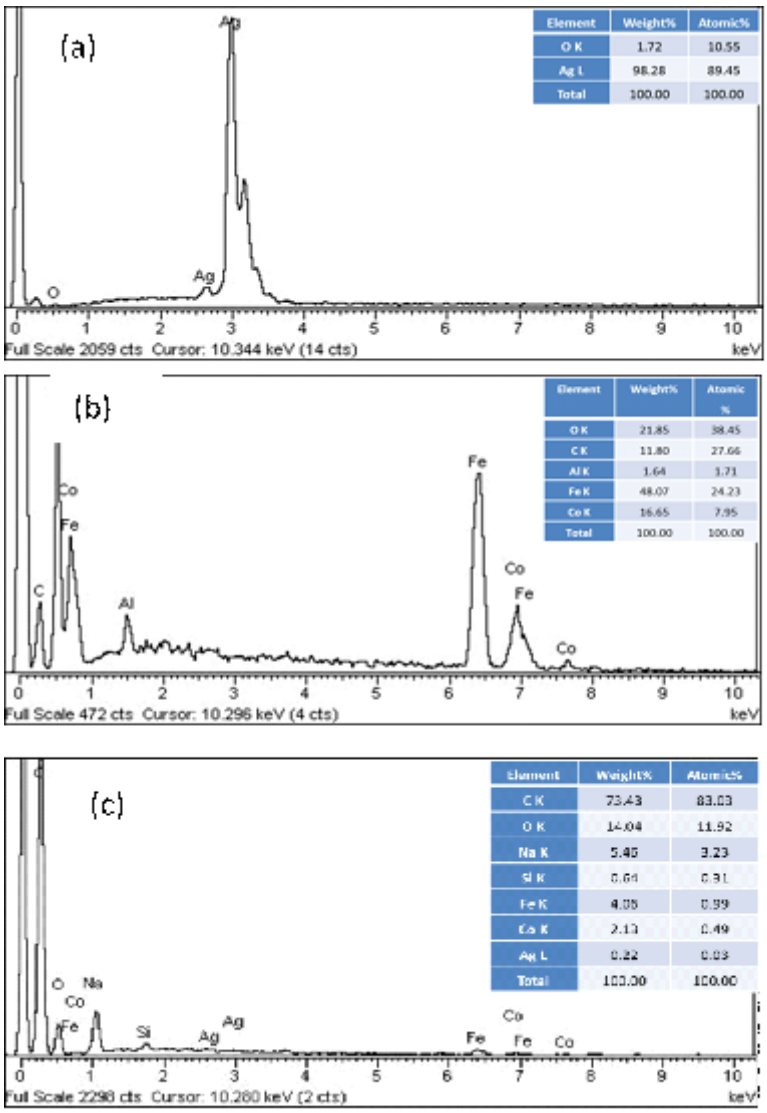

Figure 5

EDX spectra: a) Ag_2O, b) $CoFe_2O_4$ and c) $Ag_2O/CoFe_2O_4$/rGO respectively

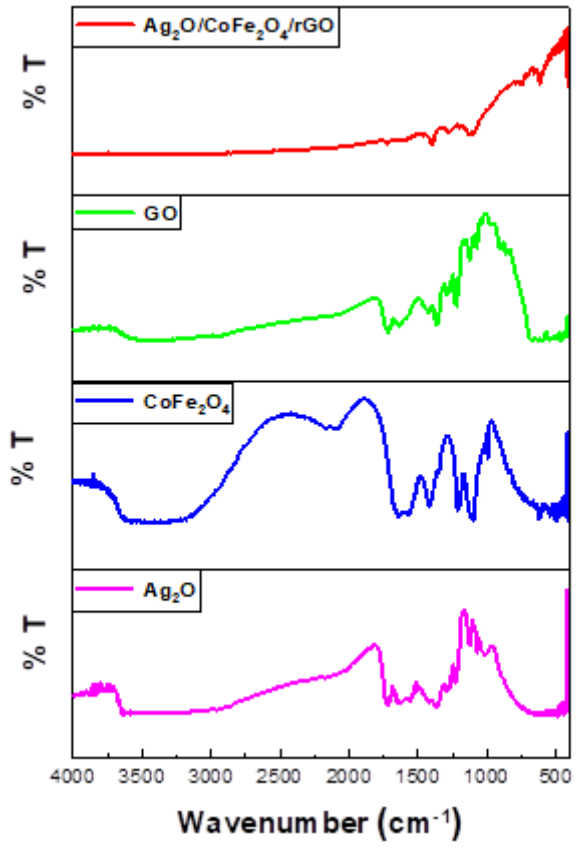

Figure 6

FTIR spectra of Ag_2O (pink), $CoFe_2O_4$ (blue), GO (green) and $Ag_2O/CoFe_2O_4$/rGO (red)

Figure 7

Bacterial activity of (a) Ag_2O, (b) $CoFe_2O_4$ (c) $Ag_2O/CoFe_2O_4$/rGO against *S. aureus* and (d) Ag_2O, (e) $CoFe_2O_4$ (f) $Ag_2O/CoFe_2O_4$/rGO against *E.coli* respectively